Jurnal Tribologi 35 (2022) 50-67

MYTRIBOS Malaysian Tribology Society

Jurnal Tribologi

Website : jurnaltribologi.mytribos.org e-issn: 2289-7232

A numerical algorithm for grease-lubricated point contact at different regimes of lubrication

Nur Aisya Affrina Mohamed Ariffin [1], Hooi Hwang Ang [1], Siti Hartini Hamdan [2], Haris Ahmad Israr Ahmad [1], William Woei Fong Chong [1,3*]

[1] Faculty of Mechanical Engineering, Universiti Teknologi Malaysia, 81310 UTM Skudai, Johor, MALAYSIA.
[2] Bio-Engineering Technology Department, University Kuala Lumpur Malaysian Institute of Chemical & Bioengineering Technology (UniKL MICET), MALAYSIA.
[3] Automotive Development Centre (ADC), Institute for Vehicle System & Engineering (IVeSE), Universiti Teknologi Malaysia, MALAYSIA.
*Corresponding author: william@utm.my

KEYWORDS

Grease
Reynolds equation
Rough surface
Friction
Lubrication

ABSTRACT

The transportation sector has been emphasizing the electrification of vehicles to promote decarbonization, with most of the frictional losses from the electric vehicle originating from 100 over rolling bearings instead of the internal combustion engine. The main concern now is the bearing system's failure due to wrong grease selection, missing relubrication, and rupturing of the lubrication film due to the high rotational speed of the bearings in the electric vehicle. Therefore, in this study, a grease lubrication problem of a point contact is numerically presented at different regimes of lubrication. A modified Reynolds equation mathematical model, considering plug-flow formation, is derived for the grease-lubricated conjunction to solve the film thickness and pressure distribution at the lubricated contact. The film thickness and pressure distribution profile are studied under two different factors: sliding velocity and applied load. The solution is integrated with the Greenwood and Tripp rough surface contact model. The predicted friction correlates with the friction test conducted through Stribeck-like analysis using a ball-on-disk tribometer. Thus, with proper adaptation, the proposed numerical algorithm provides a fundamental platform capable of aiding the grease selection used in electric vehicles.

Received 10 November 2021; received in revised form 31 December 2021; accepted 19 January 2022.
To cite this article: Mohamed Ariffin et al. (2022). Numerical algorithm for elastohydrodynamic lubrication of grease-lubricated contact. Jurnal Tribologi 35, pp.50-67.

1.0 INTRODUCTION

Since they were formed million years ago, fossil fuels have vastly been consumed as a form of energy, leading to their depletion in less than 100 years from now. As a substitute, natural oil, gas, and coal are used, but congruent to the effect of fossil fuels consumption, these energy sources take a toll on the environment, especially by emitting CO_2 gas, which leads to climate change. Interestingly, only 17.5% of the total fuel energy is used move a passenger car (Chong et al., 2018), with most of the fuel energy being wasted to overcome thermal and frictional losses. To relieve the dependency on fossil fuels, decarbonization of the transportation sector mainly hinges on developing energy-efficient vehicles, with much effort being emphasized on the electrification of vehicles. Such initiative is beneficial in terms of decarbonization via reducing/removing the combustion process of fossil fuels. By resorting to electrification, CO_2 emissions for passenger cars are estimated to reduce by 4.5 times when compared with those running on internal combustion engines (Holmberg and Erdemir, 2019). From an energy point of view, frictional losses of electric vehicles are also significantly reduced due to removing the internal combustion engine, one of the significant frictional losses' contributors.

However, the challenges arising from frictional losses in electric vehicles are very different from vehicles operating on internal combustion engines because, in an electric vehicle, most of the frictional losses originate from 100 over rolling bearings (Lugt, 2016) being used in the vehicle. About 80-90% of these rolling bearings are lubricated by grease (Lugt, 2016). The lubricating mechanisms of grease are complex when compared with typical lubricating oil. The lubricity of greases is imparted in two (2) phases: 1) churning and 2) bleeding. The churning phase begins when the bearing system is freshly greased, during which fully flooded condition is present. At this phase, the lubricating grease will be entrained into the confined region by sliding or rolling the bearing elements. A saturation of grease flow will be achieved after a certain run-in period, where the supply of lubricating grease no longer takes place. After this, the bleeding phase begins. During this phase, the lubricating oil supply will be released by the grease trapped within the confined region via phase separation.

Grease has proven to satisfy the work of minimizing friction and wear by feeding them into the contact zone between the moving parts (Zhu and Neng, 1988) due to its good anti-corrosion properties and natural sealing ability (Cen et al., 2014). However, the recently increased utilization of electric vehicles has revealed significant knowledge gaps in already established bearing technologies, especially those lubricated with grease. Instead of concerns related to the number of frictional losses, approximately 40-60% of electric motor failures have been reported to be attributed to the premature failure of the bearing system (Farfan-Cabrera, 2019) due to wrong grease selection and missing relubrication (Walther and Holub, 2014). On top of this, the electric motors adopted in electric vehicles have high rotational speeds up to 16,000 rev/min (Willwerth and Roman, 2013), which could induce temperature high enough to break down the lubrication film in the bearing system possibly.

Commonly, elastohydrodynamic lubrication (EHL) theory has been used as an interpretive theory of grease lubrication to determine the minimum film thickness (Yoo and Kim, 1997). Minimum oil film thickness remains one of the essential factors in the designing stage of the machinery parts to avoid direct contact with surfaces. Thus, appropriate minimum film thickness needed to be obtained and maintained to ensure minimal friction. Throughout the years, many numerical solutions and analyses involving theoretical and experimental studies of EHL grease have been made (Zhu and Neng, 1988). Kauzlarich and Greenwood (1972) proposed the earliest attempt using the Hershel-Bulkley model and Grubin theory, which obtained the characterization

of grease. Wada et al. (1977) attempted to model using Bingham model but only limited to Bingham solid. Jonkisz and Krzeminski-Freda (1982), Zhu and Neng (1988), and Cheng (1994) obtained a numerical solution of EHL problems with Herschel-Bulkley model grease and compared it with experimental results. Meanwhile, Dong and Qian (1988) attempted to solve for EHL problem using the Baur model.

The solutions obtained from previous models consider EHL and stop at obtaining the minimum film thickness and other parameters, such as starvation and squeeze. Most reported numerical solutions also lack the focus on friction force estimation of grease-lubricated contacts, which could comprise boundary and viscous shear components when operating at mixed and boundary lubrication regimes. To consider these friction components, rough surface contact analysis must be implemented. Typically, there are two (2) general approaches for rough surface contact analysis: stochastic and deterministic approaches. The stochastic approach adopted in literature is often derived based on the Greenwood and Williamson (1966) model. For such stochastic approaches, it is often assumed that a Gaussian distribution of asperity contact heights exists when the asperities of opposing surfaces are in contact.

On the other hand, deterministic approaches would consider the physical roughness of the surface, allowing for the immediate consideration of surface asperity height changes in the analysis, as reported by Wang et al. (2011). It is mentioned that surface asperities deform differently, resulting in the roughness inside the highly loaded contact region being different from the measured roughness (Wang et al., 2011). However, due to the random nature of surface roughness, adopting a deterministic approach could limit the findings to only the investigated surface topography. On the other hand, a stochastic approach, even though being statistical, could still be useful in producing a more generic rough surface contact solution.

Therefore, in this paper, a grease lubrication problem of a point contact is numerically presented by deriving a modified Reynolds equation capable of simulating conditions between EHL and boundary lubrication regimes. As a first approximation, a stochastic approach based on the Greenwood and Tripp (1970) rough surface contact model is adopted to consider the prevailing boundary interactions at mixed and boundary lubrication regimes. A friction test is conducted to validate the numerical model to obtain experimental data through Stribeck-like analysis using a ball-on-disk tribometer. It is expected that such a numerical model could provide a fundamental platform, capable of aiding the grease selection used in electric vehicles.

2.0 METHODOLOGY

2.1 Numerical Approach

As a first approximation, the numerical solution in the present study considers pure sliding contact. For the numerical model, the film thickness, $h(x, y)$ is taken to be a summation of three components, which are the initial film thickness, h_0, the undeformed geometry, $S(x, y)$ and the local deformation, $\delta(x, y)$. The equation can be expressed as below (Chong et al., 2019):

$$h(x, y) = h_0 + S(x, y) + \delta(x, y) \quad (1)$$

Where:

$$\mathrm{S(x,y)} = \frac{\mathrm{x}^2}{2\mathrm{R_x}} + \frac{\mathrm{y}^2}{2\mathrm{R_y}} \quad ; \; \delta(x,y) = \frac{2}{\pi E}\sum_{i=1}^{n_x}\sum_{j=1}^{n_y} p_{i,j} D_{m,n}$$

The term E is the composite elastic modulus while $D_{m,n}$ is the influence coefficient and $p_{i,j}$ is the nodal pressure. The formulas are given as below (Karthikeyan et al., 2010):

$$\frac{2}{E} = \left(\frac{1-{\nu_1}^2}{E_1} + \frac{1-{\nu_2}^2}{E_2}\right)$$

$$D_{m,n} = (\bar{y}-\bar{a})ln\left[\frac{(\bar{x}-\bar{b}) + \sqrt{(\bar{y}-\bar{a})^2 + (\bar{x}-\bar{b})^2}}{(\bar{x}+\bar{b}) + \sqrt{(\bar{y}-\bar{a})^2 + (\bar{x}+\bar{b})^2}}\right]$$

$$+ (\bar{y}+\bar{a})ln\left[\frac{(\bar{x}+\bar{b}) + \sqrt{(\bar{y}+\bar{a})^2 + (\bar{x}+\bar{b})^2}}{(\bar{x}-\bar{b}) + \sqrt{(\bar{y}+\bar{a})^2 + (\bar{x}-\bar{b})^2}}\right]$$

$$+ (\bar{x}+\bar{b})ln\left[\frac{(\bar{y}+\bar{a}) + \sqrt{(\bar{y}+\bar{a})^2 + (\bar{x}+\bar{b})^2}}{(\bar{y}-\bar{a}) + \sqrt{(\bar{y}-\bar{a})^2 + (\bar{x}+\bar{b})^2}}\right]$$

$$+ (\bar{x}-\bar{b})ln\left[\frac{(\bar{y}-\bar{a}) + \sqrt{(\bar{y}-\bar{a})^2 + (\bar{x}-\bar{b})^2}}{(\bar{y}+\bar{a}) + \sqrt{(\bar{y}+\bar{a})^2 + (\bar{x}-\bar{b})^2}}\right]$$

$$m = |k-i|; n = |l-j|; \bar{b} = \frac{\Delta x}{2}; \bar{a} = \frac{\Delta y}{2}$$

$$\bar{x} = x_{k,l} - x_{i,j} = m\Delta x; \bar{y} = y_{k,l} - y_{i,j} = n\Delta y$$

Table 1 are the parameters for the grease and base oil properties. In the present study, the viscosity-pressure, $\phi(p)$ and yield stress-pressure, $\mu(p)$ relations are described using Roelands model (Yoo and Kim, 1997). Considering the influence of contact pressure, p, they can be expressed as follow:

$$\phi(p) = \phi_0 \mathrm{e}^{\ln(\eta_o)+9.67}[-1 + (1 + 5.1\times10^{-9}p)^{\mathrm{ZV}}] \quad (2)$$

$$\mu(p) = \mu_0 \mathrm{e}^{\ln(\tau_o)+9.67}[-1 + (1 + 5.1\times10^{-9}p)^{\mathrm{ZS}}] \quad (3)$$

Where:

$$ZV = \frac{\alpha}{5.1 \times 10^{-9} \ln(\eta_o + 9.67)}$$

$$ZS = \frac{\alpha}{5.1 \times 10^{-9} \ln(\tau_o + 9.67)}$$

Meanwhile, the density-pressure equation, $\rho(p)$ can be expressed as (Chong et al., 2013, 2014):

$$\rho(p) = \rho_o \left[1 + \frac{0.6 \times 10^{-9} p}{1 + 1.7 \times 10^{-9} p}\right] \quad (4)$$

Table 1: Grease and Base Oil Properties

Parameter	Symbol	Value	Unit
Grease viscosity at zero pressure	ϕ_0	0.34	Pa.s
Pressure-viscosity coefficient	α	4.83×10^{-8}	Pa^{-1}
Yield shear stress	μ_0	800	Pa

When the yield shear stress, μ_0 is exceeded, the shear thinning layer, h_a begins to form. However, when the yield shear stress is not exceeded, the plug flow dominates. The phenomena simulated, where the plug thickness, h_p plays a significant role in influencing lubrication, can be represented by (Karthikeyan et al., 2010):

$$h_p = \frac{2\mu_0}{\sqrt{\left(\frac{dp}{dx}\right)^2 + \left(\frac{dp}{dy}\right)^2}} \quad (5)$$

The relationship between the velocity of the shear thinning layer, u_b and the plug flow, u_p is represented by the equation below (Karthikeyan et al., 2010):

$$u_p = u_b - \left(\frac{\mu_0}{\phi h_p}\right)\frac{1}{4}(h - h_p)^2 \quad (6)$$

Table 2: Simulated operating conditions.

Parameter	Symbol	Value	Unit
Sliding velocity	u_b	0.04-4	m/s
Applied normal load	W	10-50	N
Elastic Modulus - wear disk	E_1	210	GPa
Elastic Modulus - ball	E_2	210	GPa
Poisson's ratio - wear disk	ν_1	0.27	-
Poisson's ratio - ball	ν_2	0.27	-

For the present study, a 2-D modified Reynolds equation is adopted as given below to consider the plug flow formation along the grease lubricated conjunction. A simplified Herschel-Bulkley assumption is adopted, where Herschel-Bulkley index, n is taken to be unity to consider grease as a Bingham solid. With such an assumption, when the contact pressure reaches a maximum value at the centre of the contact, the lubricant would solidify and adhere to the opposing surfaces. Table 2 summarises the parameters used in the present simulation. The equation can be expressed as below (Karthikeyan et al., 2010):

$$\frac{\partial}{\partial x}\left(\frac{\rho h_a^3}{\Phi}\frac{\partial p}{\partial x}\right)+\frac{\partial}{\partial y}\left(\frac{\rho h_a^3}{\Phi}\frac{\partial p}{\partial y}\right)=12\left[\frac{\partial}{\partial x}\rho\left(hu_b-h_p u\right)+\frac{\partial}{\partial x}(\rho h)\right] \tag{7}$$

Where:

$$\mathrm{h_a}=\mathrm{h}-\mathrm{h_p};\mathrm{u}=\mathrm{u_b}-\mathrm{u_p}$$

Substituting the dimensionless parameters into equation (7), the equation can be expressed as below:

$$\frac{\partial}{\partial X}\left(\frac{\bar{\rho}{H_a}^3}{\Phi}\frac{\partial P}{\partial X}\right)+\frac{\partial}{\partial \mathrm{Y}}\left(\frac{\bar{\rho}\mathrm{H_a}^3}{\Phi}\frac{\partial \mathrm{P}}{\partial \mathrm{Y}}\right)=\Psi\left[\frac{\partial}{\partial \mathrm{X}}\bar{\rho}\left(\mathrm{HU_b}-\mathrm{H_p U}\right)+\frac{\mathrm{R_x}}{\mathrm{b}}(\bar{\rho}\mathrm{S}^*)\right] \tag{8}$$

Where:

$$\Psi=\frac{12\mathrm{u_b}\phi_0(\mathrm{R_x})^2}{\mathrm{P_h b}^3};\ \mathrm{S}^*=\frac{\frac{\partial \mathrm{h}}{\partial \mathrm{t}}}{\mathrm{u_b}}$$

The dimensionless parameters are given below:

$$X=\frac{x}{b};Y=\frac{y}{a};\bar{\rho}=\frac{\rho}{\rho_o};H=\frac{hR_x}{b^2};H_p=\frac{h_p R_x}{b^2};H_a=\frac{h_a R_x}{b^2};P=\frac{p}{p_h};\bar{\eta}=\frac{\eta}{\eta_o}$$

To setup the iterative algorithm, the finite difference method is applied to equation (8), giving the following generic expressions:

$$\mathrm{A}\ +\ \mathrm{B}\ =\Psi\left[\mathrm{C}+\frac{\mathrm{R_x}}{\mathrm{b}}(\bar{\rho}\mathrm{S}^*)\right] \tag{9}$$

It is to note that the central finite difference method is applied to LHS of equation (9) while backward finite difference method is applied to the RHS of equation (9) (Chong and De la Cruz, 2014). The terms A, B and C are represented by the following equations:

$$A = \frac{1}{2\Delta X^2}\left[\left(\frac{\bar{\rho}H_a^3}{\Phi}\right)_{i,j} + \left(\frac{\bar{\rho}H_a^3}{\Phi}\right)_{i-1,j}\right].P_{i-1,j} - \frac{1}{2\Delta X^2}\left[\left(\frac{\bar{\rho}H_a^3}{\Phi}\right)_{i+1,j} + 2\left(\frac{\bar{\rho}H_a^3}{\Phi}\right)_{i,j} + \left(\frac{\bar{\rho}H_a^3}{\Phi}\right)_{i-1,j}\right].P_{i,j} + \frac{1}{2\Delta X^2}\left[\left(\frac{\bar{\rho}H_a^3}{\Phi}\right)_{i+1,j} + \left(\frac{\bar{\rho}H_a^3}{\Phi}\right)_{i,j}\right].P_{i,j}$$

$$B = \frac{1}{2\Delta Y^2}\left[\left(\frac{\bar{\rho}H_a^3}{\Phi}\right)_{i,j} + \left(\frac{\bar{\rho}H_a^3}{\Phi}\right)_{i-1,j}\right].P_{i-1,j} - \frac{1}{2\Delta Y^2}\left[\left(\frac{\bar{\rho}H_a^3}{\Phi}\right)_{i+1,j} + 2\left(\frac{\bar{\rho}H_a^3}{\Phi}\right)_{i,j} + \left(\frac{\bar{\rho}H_a^3}{\Phi}\right)_{i-1,j}\right].P_{i,j} + \frac{1}{2\Delta Y^2}\left[\left(\frac{\bar{\rho}H_a^3}{\Phi}\right)_{i+1,j} + \left(\frac{\bar{\rho}H_a^3}{\Phi}\right)_{i,j}\right].P_{i,j}$$

$$C = \frac{(\bar{\rho}HU_b)_{i,j} - (\bar{\rho}HU_b)_{i-1,j}}{\Delta X} - \frac{(\bar{\rho}HU_b)_{i,j} - (\bar{\rho}HU_b)_{i-1,j}}{\Delta X}$$

Equation (9) is then rearranged to form the residual term, $F_{i,j}$ as follow:

$$F_{i,j} = A + B - \Psi\left[C + \frac{R_x}{b}(\bar{\rho}S^*)\right] \tag{10}$$

By applying the Taylor's expansion series, the following equation is obtained:

$$\bar{F}_{i,j} = F_{i,j} + \left[\frac{\partial F_{i,j}}{\partial P_{i-1,j}}\right]\Delta P_{i-1,j} + \left[\frac{\partial F_{i,j}}{\partial P_{i+1,j}}\right]\Delta P_{i+1,j} + \left[\frac{\partial F_{i,j}}{\partial P_{i,j-1}}\right]\Delta P_{i,j-1}\backslash + \left[\frac{\partial F_{i,j}}{\partial P_{i,j+1}}\right]\Delta P_{i,j+1} + \left[\frac{\partial F_{i,j}}{\partial P_{i,j}}\right]\Delta P_{i,j} + Err \tag{11}$$

The truncating error, *Err* is small and can be neglected as long as the numerical iteration converges. By approximating $F_{i,j} \approx 0$, equation (10) can be rearranged in terms of the change in contact pressure, $\Delta P_{i,j}$ as follow:

$$\Delta P_{i,j} = \frac{-F_{i,j} + \left[\frac{\partial F_{i,j}}{\partial P_{i-1,j}}\right]\Delta P_{i-1,j} - \left[\frac{\partial F_{i,j}}{\partial P_{i+1,j}}\right]\Delta P_{i+1,j} - \left[\frac{\partial F_{i,j}}{\partial P_{i,j-1}}\right]\Delta P_{i,j-1} - \left[\frac{\partial F_{i,j}}{\partial P_{i,j+1}}\right]\Delta P_{i,j+1}}{\frac{\partial F_{i,j}}{\partial P_{i,j}}}$$

The partial derivative terms in the form of $\frac{\partial F_{i,j}}{\partial P_{i,j}}$,j represented in the simplified forms as below:

$$J[0] = \frac{\partial F_{i,j}}{\partial P_{i+1,j}}; J[1] = \frac{\partial F_{i,j}}{\partial P_{i-1,j}}; J[2] = \frac{\partial F_{i,j}}{\partial P_{i,j+1}}; J[3] = \frac{\partial F_{i,j}}{\partial P_{i,j-1}};$$

$$J[4] = \frac{\partial F_{i,j}}{\partial P_{i,j}}; J[5] = F_{i,j}$$

The Jacobian terms are used to iteratively solve for equation (10) by adopting the Gauss-Seidel iteration approach (Chong et al., 2021). During the iterative process, the contact pressure is updated using the under-relaxation method as being expressed below, where Ω is the relaxation factor.

$$\Delta P_{i,j}^{n} = P_{i,j}^{n-1} + \Omega \Delta P_{i,j}^{n} \tag{12}$$

The iteration is continued until the pressure convergence criterion is archived. The contact pressure at the inlet and outlet of the contact is fixed at atmospheric pressure. For the present study, the value for Ω is set as 1 × 10−3. The equation for the convergence criterion is given as:

$$\frac{\sum_{i=1}^{nx}\sum_{j=1}^{ny}\left|P_{i,j}^{n} - P_{i,j}^{n-1}\right|}{\sum_{i=1}^{nx}\sum_{j=1}^{ny}P_{i,j}^{n}} \leq \varepsilon_p \tag{13}$$

In equation (13), ε_p is set to be 1×10^{-5} in the present study. When the pressure is obtained, the load applied can be calculated by integrating the contact pressure towards the contact area as in equation below:

$$W = \int p \, . \, dA \tag{14}$$

The load obtained can then be used to determine the film thickness based on the load-balance approach where the initial film thickness, h_0 in equation (1) is updated until the load convergence criterion is achieved. In present study, the load convergence is given in equation (15) where ε_w is set to be 1×10^{-2} and W_{set} is the desired load.

$$\frac{W - W_{set}}{W_{set}} \leq \varepsilon_w \tag{15}$$

To assist the understanding of the flow of the modified Reynolds solution, the flowchart in Figure 1 is presented.

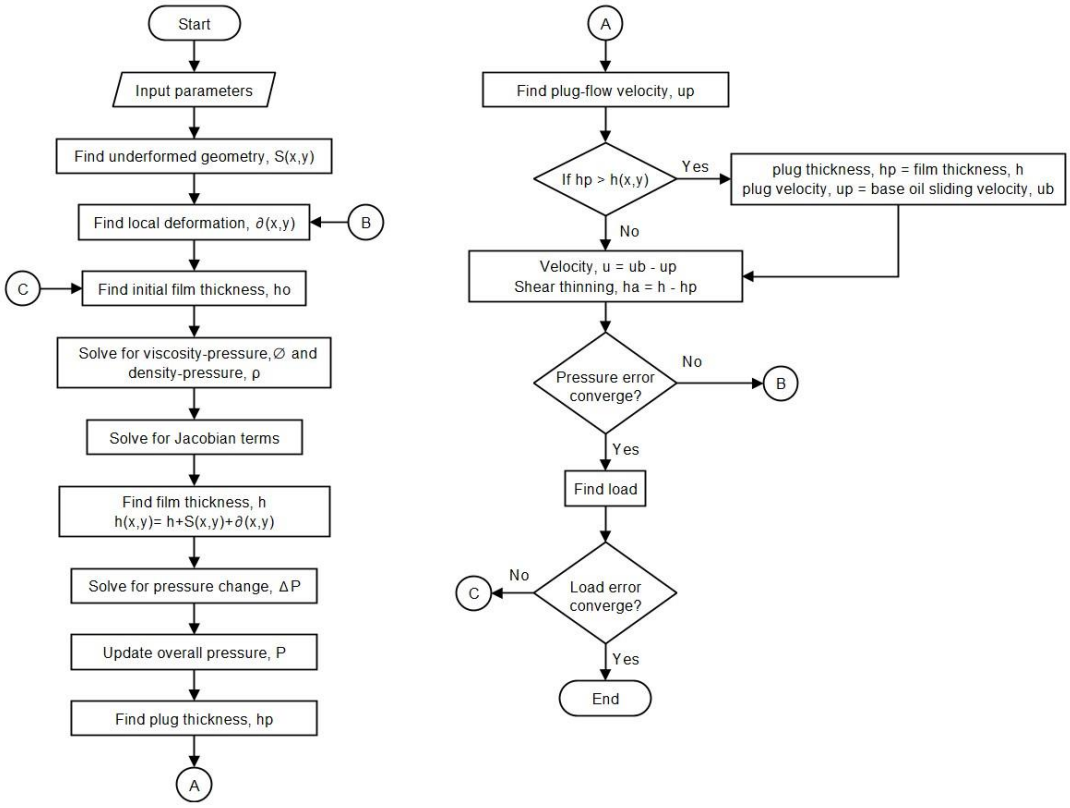

Figure 1: Flow of modified Reynolds solution.

The rough surface contact model following Greenwood and Tripp's (1970) assumption is adopted for the present study. The model, considering the contact between two rough plane surfaces, determines the extent of surface asperity interactions based on the separation parameter, λ. The model considers the surface asperities when in contact to be Gaussian distributed. From the rough surface contact model, the total friction force is taken to be the summation of the boundary friction, F_B and viscous friction, F_V components, given as follow (Ng et al., 2018):

$$F_T = F_B + F_V \tag{16}$$

The boundary friction force can be formulated using the equation below (Chong et al., 2019):

$$F_B = \tau_0 A_a + mP_a \tag{17}$$

Where τ_0 is the Eyring shear stress of the lubricant oil, where m is the pressure coefficient of the boundary. On the other hand, the viscous friction force can be determined using the following equation (Chong et al., 2019):

$$F_V = \tau_V (A - A_a) \tag{18}$$

In the case where the viscous shear, τ_V is non-Newtonian, this domain can be determined using the Eyring shear stress. When $\tau_V \leq \tau_0$, the Newtonian, τ_V is calculated as:

$$\tau_V = \frac{\eta \upsilon}{h_0} \tag{19}$$

Otherwise, the non-Newtonian, τ_V is calculated as follow:

$$\tau_V = \tau_0 + \gamma p \tag{20}$$

Where γ is the slope of the oil limiting shear stress-pressure relation and p is the lubricant contact pressure. For the adopted rough surface contact model, the asperity area, A_a and the load by asperity, P_a are estimated by the equations below (Teodorescu et al., 2003):

$$A_a = \pi^2(\zeta\beta\sigma)^2 A F_2(\lambda) \tag{21}$$

$$P_a = \frac{8\sqrt{2}}{15}\pi(\zeta\beta\sigma)^2\sqrt{\frac{\sigma}{\beta}}EAF_{5/2}(\lambda) \tag{22}$$

Where the terms λ is the separation parameter, σ is the asperity of the surface area, E is the composite elastic modulus and F (λ) are the statistical functions given below (Chong et al., 2019):

$$F_2(\lambda) = -0.116\lambda^3 + 0.4682\lambda^2 - 0.7949\lambda + 0.4999 \tag{23}$$

$$F_{5/2}(\lambda) = -0.1922\lambda^3 + 0.721\lambda^2 - 1.0649\lambda + 0.6163 \tag{24}$$

$$\lambda = \frac{h}{\sigma} \tag{25}$$

Table 3 gives the parameters related to the rough surface contact model.

Table 3: Parameters for rough surface contact model.

Parameter	**Symbol**	**Value**	**Unit**
Composite surface roughness	σ	0.105	μm
Relationship between surface density and radius of curvature at peak with composite surface roughness	$\zeta\beta\sigma$	0.4	-
Ratio of composite surface roughness to radius of curvature at peak	σ/β	0.055	-
Eyring stress	τ_0	2.0	MPa

2.2 Experimental Approach

The friction tests are conducted using the TE-165 tribometer, manufactured by Magnum Engineers, in compliance with ASTM G99. The tribometer is configured for a ball-on-disk setup, where a 304 stainless-steel ball with a diameter of 8 mm and a JISSKD-11 tool steel wear disk are used and tested with commercially available grease of clay thickener and mineral oil as the base oil. The grease (approximately 10 g) is then spread uniformly along the wear track region on the wear disk. During the test, the stationary ball is placed 20 mm from the center of the wear disk. Before the friction test, a run-in test is conducted at 1000 rpm at 1 kg for 90 seconds.

The friction tests are then conducted with normal loads from 1 kg to 5 kg. For each selected normal load, the speed is varied between 20 rpm and 2000 rpm. With a test duration of approximately 90 seconds for each tested speed, the total sliding distance for the friction test is approximated to be 10,000 m. The prescribed procedure follows the one explained by Chong et al. (2019) for friction measurements at a wide range of lubrication regimes. The test is repeated twice, using a new set of balls and disks to ensure consistency of the friction measurements.

3.0 RESULTS AND DISCUSSION

The proposed numerical algorithm simulates a ball-on-disk contact lubricated with a commercially available grease with clay as the thickener and mineral oil as the base oil. It is to note that no extreme pressure additives are added to the selected grease. Figures 2 and 3 illustrate the contact pressure and film thickness in x- and y-direction, respectively. In the x-direction (sliding direction), the contact pressure resembles the Hertzian contact pressure at 0.04 m/s. As the sliding velocity increases up to 4 m/s, a secondary peak prevails for the contact pressure distribution in the sliding direction. The trend indicates that the contact begins to transit from boundary lubrication regime towards elastohydrodynamic lubrication regime. In Figures 2 and 3, the film thicknesses are also plotted along with the plug thickness, h_p. It is demonstrated that the plug adheres to the contact surfaces for the simulated operating conditions. This characteristic conforms to the Bingham model assumption, where the grease solidifies and adheres to the contact surfaces at the contact center and in the region of the minimum exit film. When the sliding velocity increases, the plug becomes thicker but reduces in the contact area. It would be expected that with a further increase in sliding velocity, the plug would then detach from the contacting surfaces, allowing for the base oil to dominate the lubrication performance at the contact. However, the present model would no longer be able to accurately model this scenario, which requires the adoption of the full Herschel-Bulkley fluid assumption.

The minimum film thickness of the simulated contact is given in Figure 4 for varying applied normal loads at three selected sliding velocities. For the simulated contact, the composite roughness is given as 0.105 μm. When the film thickness is comparable with the composite roughness, boundary interactions between surface asperities begin to prevail, giving rise to higher friction. From Figure 4, it is shown that at sliding velocities above 0.4 m/s, the minimum film thickness is relatively larger as compared to the composite roughness. Under this condition, the friction is expected to be dominated by the viscous shear component. However, as the sliding velocity slows down from 0.4 m/s, the minimum film thickness of the contact is closer to the composite roughness value. Eventually, at 0.04 m/s, it is, thus, expected that the boundary friction component will dominate the friction of the contact.

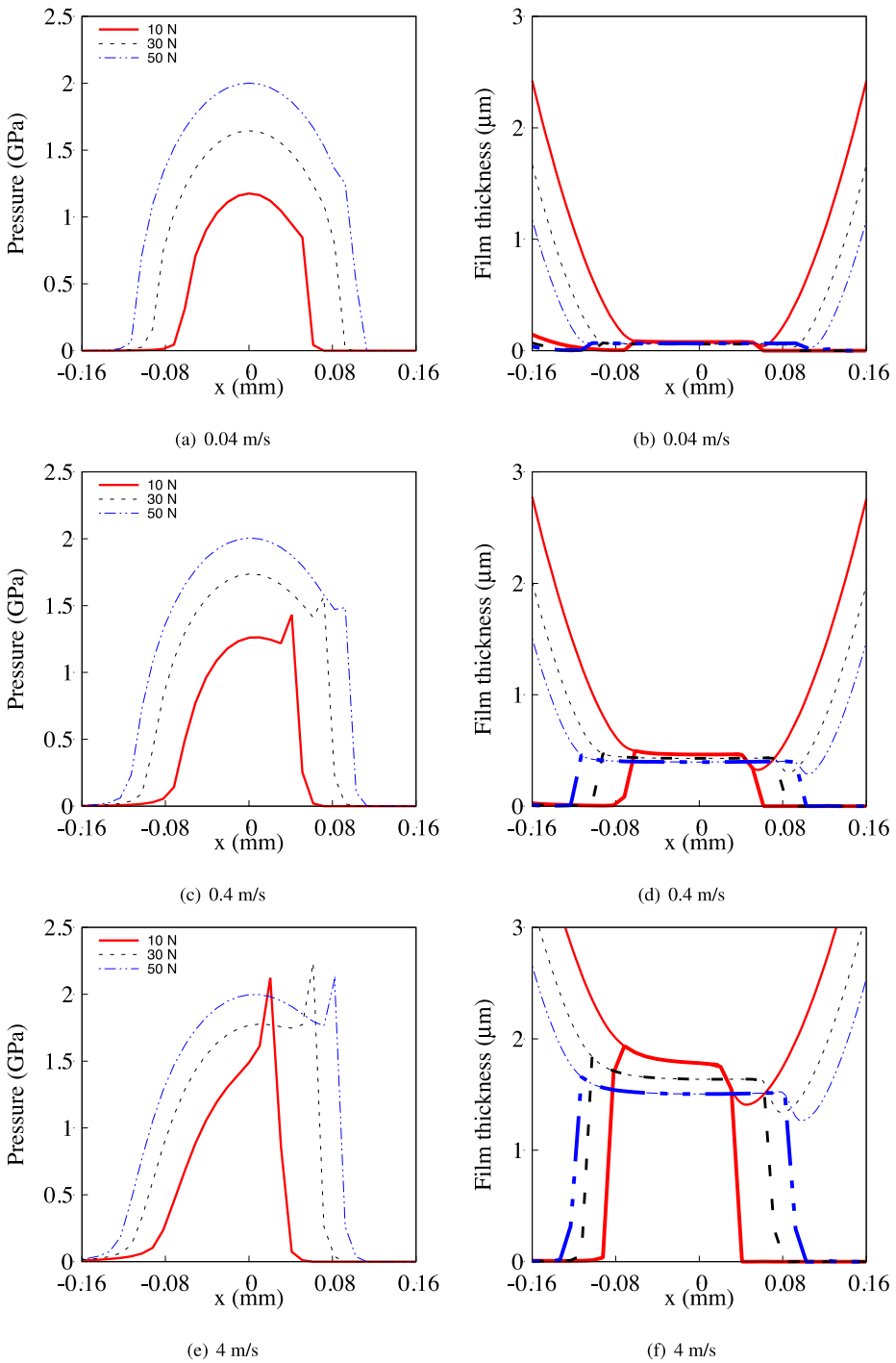

Figure 2: Contact pressure and film thickness of the simulated contact in x-direction (sliding direction).

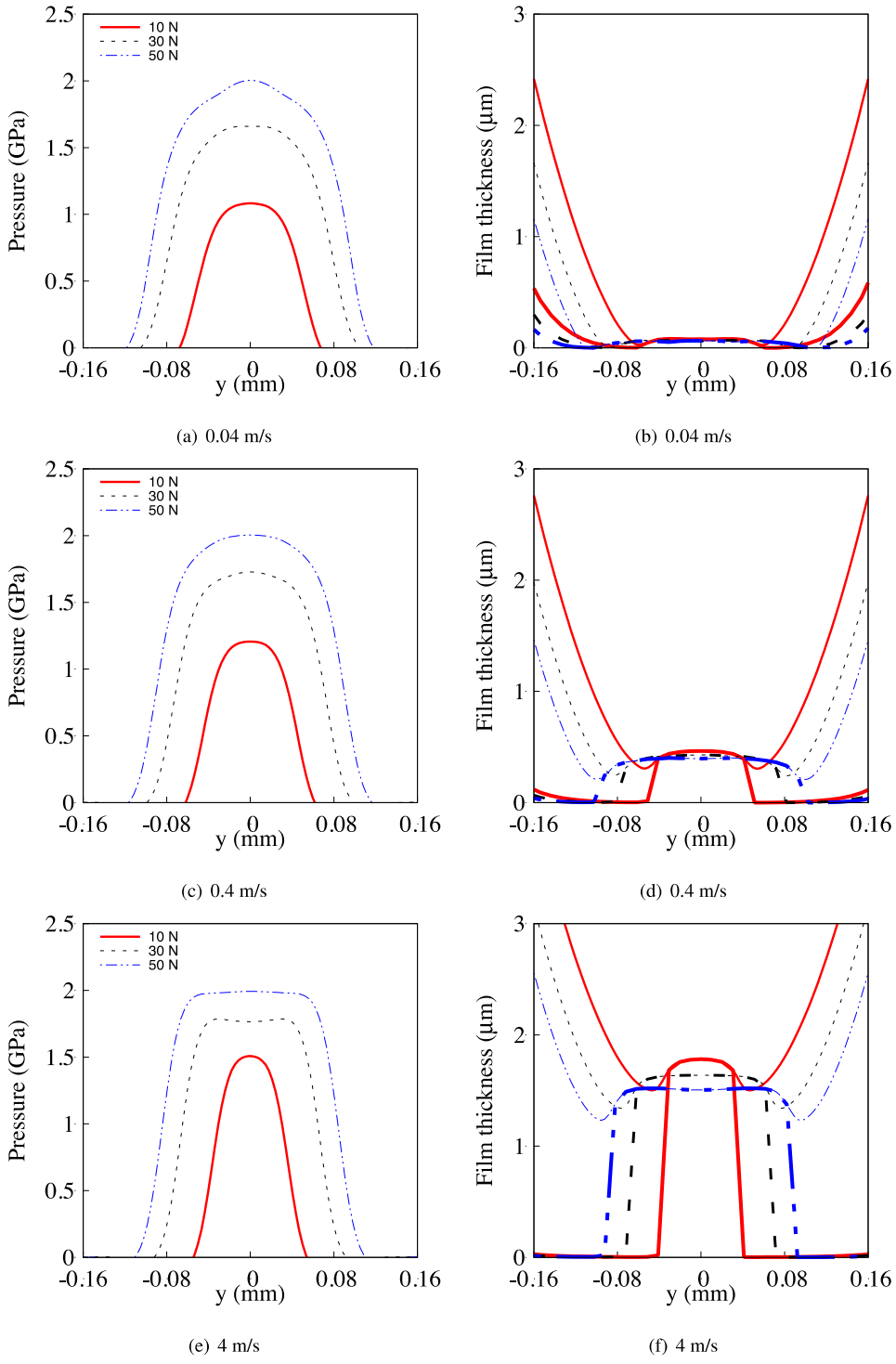

Figure 3: Contact pressure and film thickness of the simulated contact in y-direction.

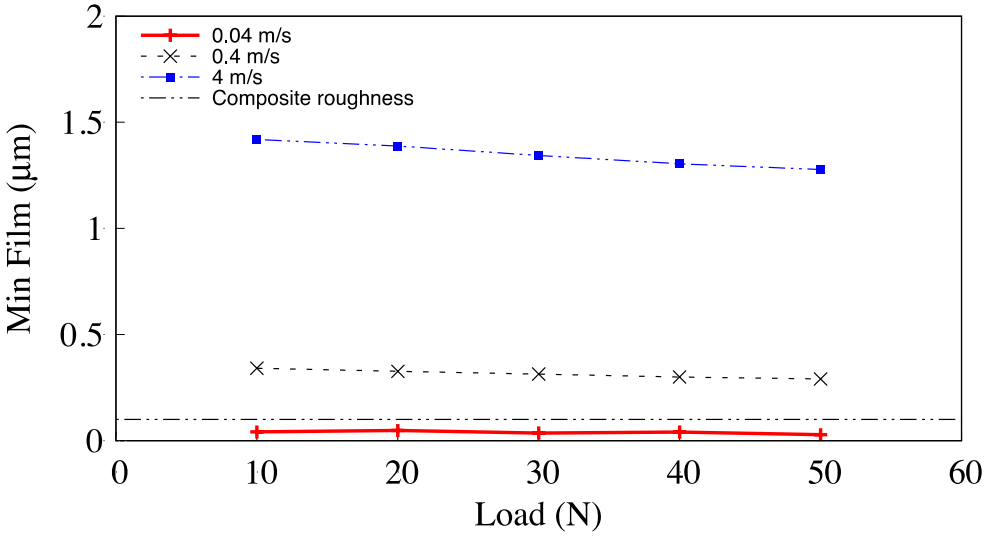

Figure 4: Minimum film thickness of the simulated contact in y-direction.

As validation of the present model, friction for the selected grease, comprising clay as thickener and mineral oil as the base oil, has been measured at different applied normal loads and sliding velocities using a ball-on-disk tribometer. For grease lubrication, under compression, the base oil trapped by the thickener would gradually be released. Typically, at faster sliding velocities, the grease lubrication has been influenced by the base oil. On the other hand, at slower sliding velocities, the grease lubrication would be affected by the properties of the thickener. Such a trend gives rise to an inverse-Stribeck curve behavior (De Laurentis, Kadiric, Lugt, and Cann, 2016). It is realized that a constant set of coefficient values for shear stress components is no longer sufficient to account for this kind of lubrication performance transition. More so, experimentally extracting such information would be tedious as the phenomenon is overly complex. Therefore, as a first approximation, the simulated friction force is fitted to the experimental data by setting a benchmark of correlation factor, R-squared of at least 0.85 at a given sliding velocity condition. Figure 5 plots the shear stress coefficients, m and γ obtained by correlating the simulated friction force with the experimentally measured values. It is to note that the coefficient m is used to determine the boundary friction component while the coefficient γ is used to determine the viscous friction component. The coefficient m can only be matched when boundary friction exists below 0.2 m/s, while the coefficient γ can only be matched when viscous friction exists above 0.1 m/s. From Figure 5, it is also demonstrated that both the boundary and viscous friction components coexist between 0.1 m/s and 0.2 m/s, giving rise to a mixed lubrication regime. Referring to Figure 4, the minimum film at a given sliding velocity is relatively constant with increasing normal load. Therefore, as a first approximation, at a given sliding velocity, the minimum film thickness predicted for across the applied normal load is averaged and given in figure 5. Figure 6 presents the predicted friction force when compared with the measured values at three selected sliding velocities. Overall, it can be observed that the simulated friction force compares relatively well with the experimentally measured values.

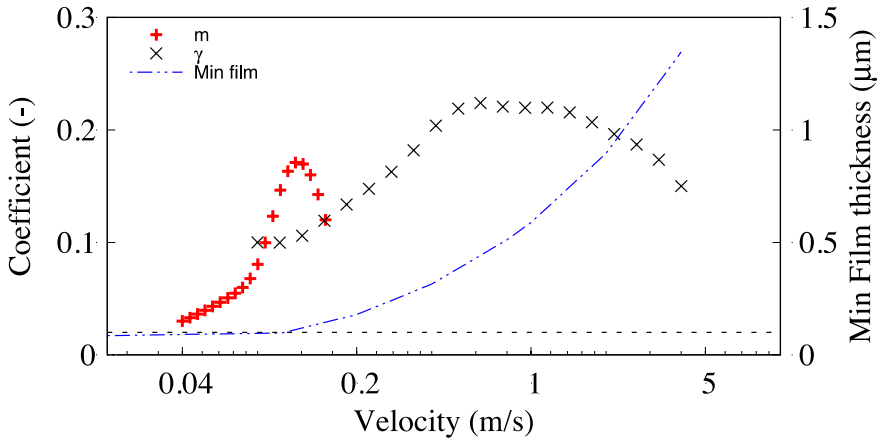

Figure 5: Shear stress related coefficients for friction prediction.

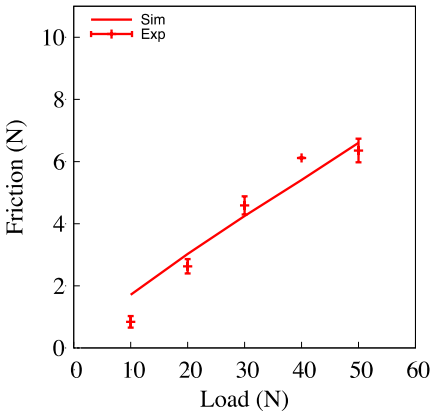

(a) 0.04 m/s (R-squared=0.989)

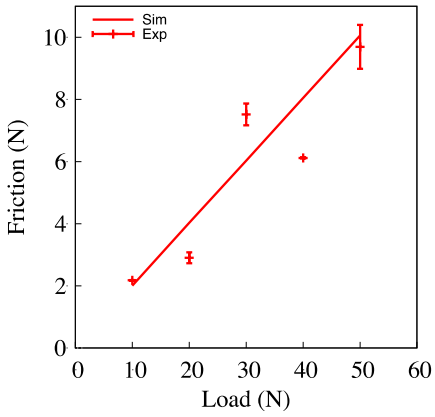

(b) 0.4 m/s (R-squared=0.968)

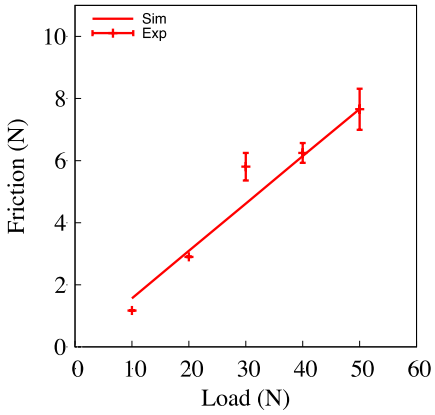

(c) 4 m/s (R-squared=0.989)

Figure 6: Friction force comparison between simulated and experimental data.

By determining the coefficient of friction (CoF) based on Figure 6, Figure 7 shows the predicted inverse-Stribeck curve for the simulated grease-lubricated contact. The predicted coefficient of friction correlates well with the experimental data with an R-squared of 0.94. This plot also shows that the proposed numerical algorithm can predict the frictional performance of a lubricated grease contact if the Bingham assumption is still valid within the selected operating conditions.

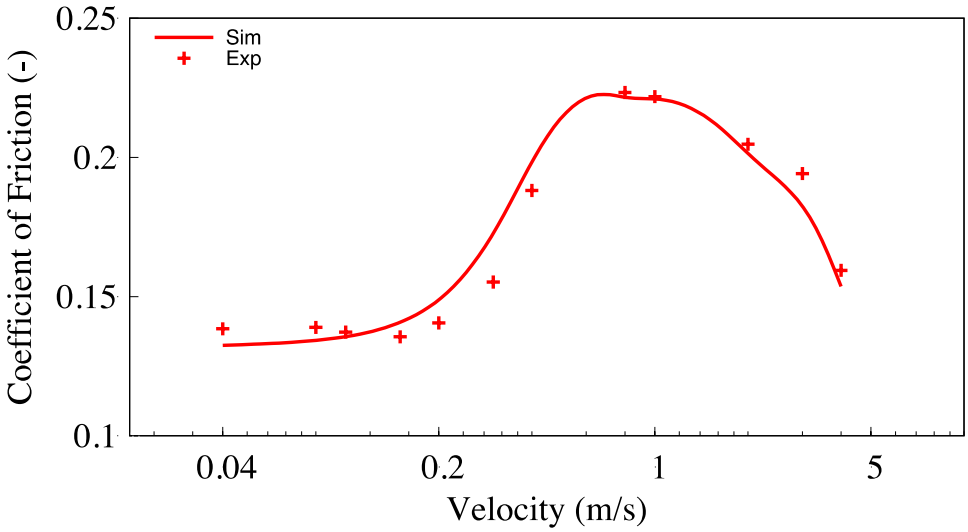

Figure 7: Inverse-Stribeck curve for the simulated grease lubricated contact.

CONCLUSIONS

In the present study, the primary purpose is to develop a numerical model of a grease lubrication problem for a point contact, capable of predicting the tribological behavior of the grease at different regimes of lubrication. It simulates the ball-on-disk contact lubricated with a commercially available grease with clay as the thickener and mineral oil as the base oil. The presented results reflected the Bingham model assumption, where the grease solidifies and sticks to the contact surfaces at the contact center and in the region of the minimum exit film. The sliding velocity affected the plug formation, which 1) it becomes thicker and reduced in the contact area when the velocity increases and 2) further increasing of the velocity may result in the detachment of the plug from the contact area, making the base oil to dominate the lubrication performance. The predicted film thickness for the varying applied load and sliding velocities are used to predict the friction force by comparing the film thickness with the composite roughness. It can be concluded that 1) the high sliding velocities give out larger minimum film thickness compared to the composite roughness, and the friction is dominated by the viscous shear component, and 2) as the velocity is slowing down, the minimum oil film thickness is closer to the composite roughness value and the boundary friction component dominates the friction.

An experimental procedure under different sliding velocities and applied loads are performed using the ball-on-disk tribometer for validation. The friction model parameters, namely the pressure coefficient of the boundary shear strength (m) and the slope of the oil limiting shear stress-pressure relation (γ), are fitted to the experimental data. Based on the presented result, it

can be observed overall that the simulated friction force compares relatively well with the experimentally measured values. The friction forces simulated and measured have been further compared using the Stribeck-like analysis, where the coefficient of friction is plotted against the varying sliding velocity. The predicted coefficient of friction correlates well with the experimental data, showing that the proposed numerical algorithm can predict the frictional performance of a lubricated grease contact given that the Bingham assumption is still valid, as reported in the literature for grease application. Thus, it can be surmised that the presented numerical algorithm prepares for a fundamental platform that can be further adapted to aid the grease selection for electric vehicle applications.

ACKNOWLEDGMENTS

The authors would like to acknowledge the support provided by the UTM Fundamental Research Grant, Universiti Teknologi Malaysia (UTM) under Project vot No. Q.J130000.3851.22H02 (PY/2015/04925).

REFERENCES

Cen, H., Lugt, P. M., & Morales-Espejel, G. (2014). On the Film Thickness of Grease-Lubricated Contacts at Low Speeds. Tribology Transactions, 57(4), 668–678.

Cheng, J. (1994). Elastohydrodynamic grease lubrication theory and numerical solution in line contacts. Tribology Transactions, 37(4), 711–718. doi: 10.1080/10402009408983350

Chong, W. W. F., & De la Cruz, M. (2014). Elastoplastic contact of rough surfaces: a line contact model for boundary regime of lubrication. Meccanica, 49(5), 1177–1191.

Chong, W. W. F., Hamdan, S. H., Wong, K. J., & Yusup, S. (2019). Modelling transitions in regimes of lubrication for rough surface contact. Lubricants, 7(9), 77.

Chong, W. W. F., Howell-Smith, S., Teodorescu, M., & Vaughan, N. D. (2013). The influence of inter-ring pressures on piston-ring/liner tribological conjunction. Proceedings of the Institution of Mechanical Engineers, Part J: Journal of Engineering Tribology, 227(2), 154–167.

Chong, W. W. F., Lee, C. T., & Lee, M. B. (2021). Simulating thermo-hydrodynamic lubrication of turbocharger journal bearing. Jurnal Tribologi, 30, 13–23.

Chong, W. W. F., Ng, J. H., Rajoo, S., & Chong, C. T. (2018). Passenger transportation sector gasoline consumption due to friction in southeast asian countries. Energy conversion and management, 158, 346–358.

Chong, W. W. F., Teodorescu, M., & Rahnejat, H. (2014). Mixed thermo-elastohydrodynamic cam–tappet power loss in low-speed emission cycles. International Journal of Engine Research, 15(2), 153–164.

De Laurentis, N., Kadiric, A., Lugt, P., & Cann, P. (2016). The influence of bearing grease composition on friction in rolling/slidi dng concentrated contacts. Tribology International, 94, 624–632.

Dong, D., & Qian, X. (1988). A theory of elastohydrodynamic grease-lubricated line contact based on a refined rheological model. Tribology International, 21(5), 261–267. doi: 10.1016/0301-679X(88)90003-5

Farfan-Cabrera, L. I. (2019). Tribology of electric vehicles: A review of critical components, current state and future improvement trends. Tribology International, 138, 473–486.

Greenwood, J. A., & Tripp, J. H. (1970). The contact of two nominally flat rough surfaces. Proceedings of the institution of mechanical engineers, 185(1), 625-633.

Greenwood, J. A., & Williamson, J. P. (1966). Contact of nominally flat surfaces. Proceedings of the royal society of London. Series A. Mathematical and physical sciences, 295(1442), 300-319.

Holmberg, K., & Erdemir, A. (2019). The impact of tribology on energy use and co2 emission globally and in combustion engine and electric cars. Tribology International, 135, 389–396.

Jonkisz, W., & Krzeminski-Freda, H. (1982). The properties of elastohydrodynamic grease films. Wear, 77(3), 277–285. doi: 10.1016/0043-1648(82)90053-9

Karthikeyan, B. K., Teodorescu, M., Rahnejat, H., & Rothberg, S. J. (2010). Thermoelastohydrodynamics of grease-lubricated concentrated point contacts. Proceedings of the Institution of Mechanical Engineers, Part C: Journal of Mechanical Engineering Science, 224(3), 683–695.

Kauzlarich, J. J., & Greenwood, J. (1972). Elastohydrodynamic lubrication with herschel-bulkley model greases. ASLE transactions, 15(4), 269–277.

Lugt, P. M. (2016). Modern advancements in lubricating grease technology. Tribology international, 97, 467–477.

Ng, Y. C., Hamdan, S. H., & Chong, W. W. F. (2018). Development of a mathematical tool to predict engine in-cylinder friction. Jurnal Tribologi, 17, 29–39.

Teodorescu, M., Taraza, D., Henein, N. A., & Bryzik, W. (2003). Simplified elasto-hydrodynamic friction model of the cam-tappet contact. SAE Technical Papers(724).

Wada, S., Hayashi, H., & Haga, K. (1977). NII-Electronic Library Service NII-Electronic Library Service. Elastodrodynamic Lubrication of a Bingham Solid, 20(139), 111–115.

Walther, H. C., & Holub, R. A. (2014). Lubrication of electric motors as defined by ieee standard 841-2009, shortcomings and potential improvement opportunities. In 2014 ieee petroleum and chemical industry technical conference (pcic) (pp. 91–98).

Wang, J., Venner, C. H., & Lubrecht, A. A. (2011). Amplitude reduction in EHL line contacts under rolling sliding conditions. Tribology international, 44(12), 1997-2001.

Willwerth, A., & Roman, M. (2013). Electrical bearing damage?a lurking problem in inverter-driven traction motors. In 2013 ieee transportation electrification conference and expo (itec) (pp. 1–4).

Yoo, J. G., & Kim, K. W. (1997). Numerical analysis of grease thermal elastohydrodynamic lubrication problems using the Herschel-Bulkley model. Tribology International, 30(6), 401–408.

Zhu, W. S., & Neng, Y. T. (1988). A theoretical and experimental study of EHL lubricated with grease. Journal of Tribology, 110(1), 38–43.